Estimating Parameters of the Structural Pilot Model Using Simulation Tracking Data

R. A. Hess[1] and J. K. Moore[2]

Dept. of Mechanical and Aerospace Engineering, University of California, Davis, Davis, CA 95616

The research to be described presents a preliminary analysis of a method for identifying a limited set of parameters from the Structural Pilot Model using data from human-in-the loop simulation tasks. Four simple controlled-element dynamics are chosen requiring pilot compensation ranging from lags to first-order leads. Then tracking data for longitudinal control of a model of a large transport aircraft is analyzed for a cruise flight condition. In all cases, the Structural Pilot Model parameters are limited to those in the proprioceptive feedback loop and the forward loop operating on visually displayed error. These parameter values determine fundamental pilot compensation and open-loop crossover frequencies. Using the identified pilot model parameters, Handling Qualities Sensitivity Functions are created for the estimation of vehicle handling qualities levels.

I. Introduction

Reference 1 discusses techniques for the estimation of human pilot dynamics in the control of time-varying systems. The methodology of Ref. 1 concentrated upon time-domain identification of pilot dynamics with an emphasis upon estimating fundamental equalization characteristics and open-loop crossover frequencies. Often in flight simulation research there is a need for establishing these characteristics and frequencies with different flight control systems designs such as the ones discussed in Ref. 2. The methodology to be discussed herein is based upon an identification technique exercised in Ref. 3 for the purpose of identifying the dynamic characteristics of the human bicycle rider, using a rider model described in Ref. 4. It will be applied here for estimating parameters of the Structural Pilot Model.[5]

II. Identification Technique

The following discussion is taken from Refs. 3 and 6. Time-domain techniques for estimating parameters of human operator models has a long lineage.[7,8] The pilot description is given by

$$\begin{aligned} \dot{x}(t) &= \mathbf{F}x(t) + \mathbf{G}u(t) \\ \eta(t) &= \mathbf{H}x(t) \end{aligned} \tag{1}$$

where **F** and **G** describe the pilot model. Here **η** is the vector of outputs and **H** is the identity matrix. Now assuming a sampling period of T and assuming a zero-order hold, Eqs. 1 can be written

$$\begin{aligned} x(kT+T) &= \mathbf{A}(\theta)x(kT) + \mathbf{B}(\theta)u(kT) + w(kT) \\ y(kT) &= \mathbf{C}(\theta)x(kT) + v(kT) \end{aligned} \tag{2}$$

Here **A(θ)** and **B(θ)** represent the state space description and **C(θ)** part of the output relation, all associated with the pilot model description. **θ** represents the unknown Structural Pilot Model parameters. The additional terms *w* and *v* represent process and measurement noise vectors, respectively. They are assumed to be sequences of zero mean white Gaussian noise. Equations 2 can, with the introduction of a Kalman filter, be transformed such that the optimal estimate of the states is given by

$$\begin{aligned} \hat{x}(kT+T,\theta) &= \mathbf{A}(\theta)\hat{x}(kT) + \mathbf{B}(\theta)u(kT) + \mathbf{K}(\theta)e(kT) \\ y(kT) &= \mathbf{C}(\theta)\hat{x}(kT) + e(kT) \end{aligned} \tag{3}$$

[1]Professor, Fellow AIAA
[2]Post-Doctoral Researcher

where **K** is the Kalman gain matrix and is a function of **A(θ)**, **C(θ)** and the covariance and cross covariance of the process and measurement noises. The matrix **K** can also be parameterized by **θ.** Thus, Eq. 3 is referred to as the *directly parameterized innovations form.* [6]

The **A** and **B** matrices are related to **F** and **G** by

$$\begin{aligned} \mathbf{A}(\theta) &= e^{\mathbf{F}(\theta)T} \\ \mathbf{B}(\theta) &= \int_{\tau=0}^{T} e^{\mathbf{F}(\theta)\tau}\mathbf{G}(\theta)d\tau \end{aligned} \tag{4}$$

With the assumption of linearity, A and B can be estimated in discrete form by

$$\begin{aligned} \mathbf{A}(\theta) &= \mathbf{I} + \mathbf{F}(\theta)T \\ \mathbf{B}(\theta) &= \int_{\tau=0}^{T} (\mathbf{I} + \mathbf{F}(\theta)\tau)\mathbf{G}(\theta)d\tau \end{aligned} \tag{5}$$

A one step ahead predictor for the innovations form is

$$\hat{y}(t|\theta) = \mathbf{C}(\theta)[q\mathbf{I} - \mathbf{A}(\theta) + \mathbf{K}(\theta)\mathbf{C}(\theta)]^{-1}[\mathbf{B}(\theta)u(t) + \mathbf{K}(\theta)y(t)] \tag{6}$$

with q being the forward shift operator. The predictor is a vector of length *p* in which each entry is a ratio of polynomials in *q*. These are transfer functions in q from the previous inputs and outputs to the current output. In general the coefficients of *q* are non-linear functions of the parameters **θ**.

A cost function can now be constructed to enable the computation of the parameters of the pilot model which provide the best fit using an optimization approach. The object here would be to minimize the error between the predicted and measured output. One first forms $\mathbf{Y_N}$, a pN x 1 vector containing all the current outputs at time kT:

$$Y_N = [y_1(1)\ldots y_p(1)\ldots y_1(N)\ldots y_p(N)]^T \tag{7}$$

In Eq, 7, *p* is the number of outputs and N is the number of samples. Organizing the predictor vector $\mathbf{Y_N(\theta)}$ the one step ahead prediction of $\mathbf{Y_N}$ given y(s) and u(s) where s ≤ t-1 yields

$$\hat{Y}_N = \left[\hat{y}_1(1)\ldots\hat{y}_1(1)\ldots\hat{y}_p(N)\ldots\hat{y}_p(N)\right]^T \tag{8}$$

The cost function then becomes the norm of the difference between $\mathbf{Y_N}$ and $\mathbf{Y_N(\theta)}$ over all *k*, i.e.,

$$V_N(\theta) = \frac{1}{pN}\,||Y_N - \hat{Y}_N(\theta)|| \tag{9}$$

The value of **θ** which minimizes the cost function is the best prediction, i.e.,

$$\hat{\theta}_N = \underset{x}{\operatorname{argmax}}\, V_N(\theta, Z^N) \tag{10}$$

where $\mathbf{Z^N}$ is the set of all measured inputs and outputs. The optimization technique is susceptible to local minima. This means that the established technique for estimating Structural Model parameters was employed to provide initial guesses for the identification procedure.[5,9] It should be noted that the in the identification procedure used herein, the noise gain matrix **K** in Eq. 3 will not be identified, but rather set to zero.

With estimation error, ε, defined as

$$\boldsymbol{\varepsilon} = \hat{\boldsymbol{Y}} - \boldsymbol{Y} \tag{11}$$

The covariance of θ can be computed as

$$\boldsymbol{\sigma^2} = \boldsymbol{\varepsilon^T \varepsilon} \tag{12}$$

As emphasized in Ref. 3, the minimization problem is not trivial and is susceptible to issues typically associated with optimization, the most important of which here are local minima. Thus, in the current application, it is essential to reduce the number of unknown parameters, a fact which serves as an introduction to the human operator modeling of Section III.

III. Simple, Single-Axis Tracking Examples

A. Tracking Tasks

Four single-axis tracking tasks were conducted with controlled-element dynamics given by

Task 1:

$$Yc_1(s) = \frac{1}{s}$$

Task 2:

$$Yc_2(s) = \frac{1}{s(s+1)}$$

Task 3:

$$Yc_3(s) = \frac{1}{[s(s+0.2)]} \tag{13}$$

Task 4:

$$Yc_4(s) = \frac{10}{(s+10)}$$

The block diagram for the compensatory task is shown below. The simulations were mechanized on a desk-top computer with MATLAB Simulink® serving as the simulation software. Reference 1 discussed the use of Simulink® as a real-time simulation set-up.

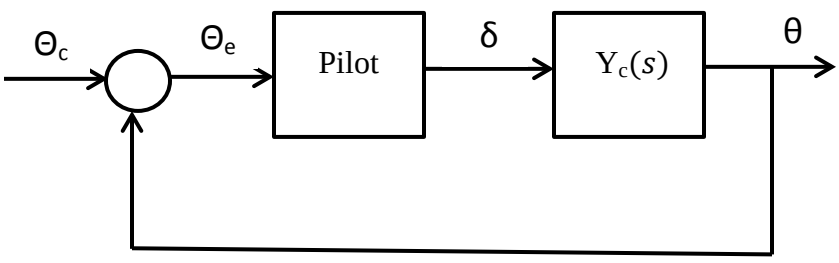

Figure 1 A block diagram of the tracking task.

The command signal θ_c (t) consisted of a sum of sinuosoids as given in Table 1.

Table 1 Command Sum of Sinusoids Frequencies

$\omega_1 = 2\pi(7/240)$ rad/sec	$\omega_7 = 2\pi(131/240)$ rad/sec
$\omega_2 = 2\pi(16/240)$ rad/sec	$\omega_8 = 2\pi(151/240)$ rad/sec
$\omega_3 = 2\pi(25/240)$ rad/sec	$\omega_9 = 2\pi(181/240)$ rad/sec
$\omega_4 = 2\pi(38/240)$ rad/sec	$\omega_{10} = 2\pi(220/240)$ rad/sec
$\omega_5 = 2\pi(61/240)$ rad/sec	$\omega_{11} = 2\pi(313/240)$ rad/sec
$\omega_6 = 2\pi(103/240)$ rad/sec	

An aircraft pitch-attitude display shown in Fig. 2 was utilized in the tasks. The RMS value of the pitch-attitude command was 0.75 deg.

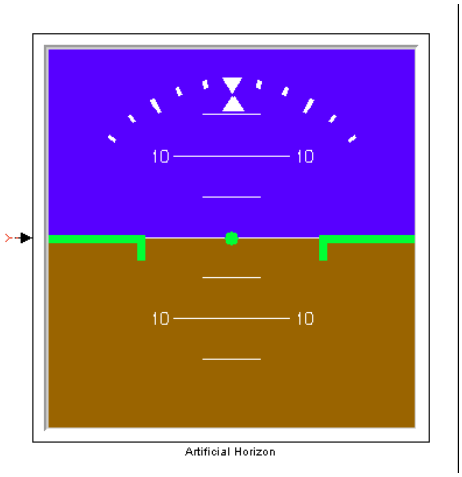

Figure 2 The pitch attitude display for the tracking task.

In each of the tasks to be described, the identification was conducted on the single run of a well-trained subject. Thus, the purpose of the study was to demonstrate the general utility of the identification approach rather than a detailed description of operator dynamics.

B. Structural Pilot Model Parameterization

The Structural Pilot Model is shown in Fig. 3.

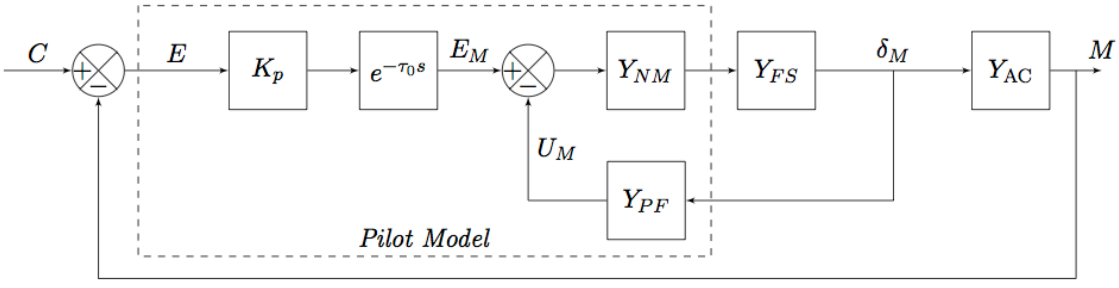

Figure 3 The Structural Pilot Model.

In the model above,

$$Y_e = K_1,\ Y_{PF} = K_2(s+K_4)/(s+K_3). \tag{14}$$

and

$$Y_{FS} = 65^2/(s^2 + 2*.707*65s + 65^2)$$
$$Y_{NM} = 100/(s^2 + 2 * .707 * 10s + 100),\ \tau_0 = 0.2 \text{ sec.} \tag{15}$$

In the identification procedure, the time delay is represented by a simple Pade approximation, i.e.,

$$e^{-\tau_0 s} = \frac{-\left(s-\frac{2}{\tau}\right)}{\left(s+\frac{2}{\tau}\right)} \tag{16}$$

In the identifications to be described, only the gains K_1 through K_4 will be identified. The rationale for this simplification is to permit concentration on the fundamental equalization capabilities of the human (generation of lead, lag, etc), and an estimation of open-loop crossover frequencies. The tracking runs involved a single, well-trained subject and were deliberately brief, being only 60 sec in duration. Of this 60 sec run, the first 30 sec were devoted to identification, and the last 30 sec to evaluation of the VAF. A word or two on the form of Eq. 14 is in order. The form was chosen so that it could accommodate the proprioceptive dynamics ($Y_{PF)}$ in evidence across a wide range of controlled element dynamics. These Y_{PF} forms range from low-frequency differentiation (Task 4) to low-frequency integration (Task 3).[5,9] The initial parameter estimates for the four tasks using the controlled elements of Eqs. 13 are given in Table 2 and were obtained by creating the Structural Pilot Model.[5,9] It is worth noting that with the four parameters of Eq. 14, the Structural Pilot Model is over-parameterized for the controlled elements in the first three tasks. This was done to allow a single four-parameter model to be used throughout the identification procedure.

Table 2 Initial Estimates for Structural Model Parameters

Task 1: $K_1 = 4.85$, $K_2 = 1.79$, $K_3 = 20$, $K_4 = 20$.
Task 2: $K_1 = 14.5$, $K_2 = 0.375$, $K_3 = 1$, $K_4 = 20$.
Task 3: $K_1 = 12.3$, $K_2 = 0.354$, $K_3 = 0.2$, $K_4 = 20$.
Task4: $K_1 = 1.68$, $K_2 = 9.49$, $K_3 = 20$, $K_4 = 0$;

C. Identification Results

Table 3 shows the identification results. The ± bounds on the identified gains define the standard deviations of parameter estimates with respect to how well the model fits the data. The column labeled VAF is the variance accounted for in the output and defined as

$$\text{VAF} = 1 - \frac{var(y_i - \hat{y}_i)}{var(y_i)} \tag{17}$$

Table 3 Identified Structural Model Parameters and VAF

K_i	VAF	K_i	VAF
Task 1: K_1 = 4.42		Task 3: K_1 = 15.2	
K_2 = 1.78		K_2 = 0.316	
	0.69		0.34
K_3 = 1.4		K_3 = 0.186	
K_4 = 0.972		K_4 = 18.2	
Task 2: K_1 = 14.4		Task 4: K_1= 1.66	
K_2 = 0.284		K_2 = 10.6	
	0.37		0.65
K_3 = 1.02		K_3 = 22.5	
K_4 = 121.8		K_4 = 0.321	

The relatively low VAFs for Tasks 2 and 3 are not atypical,[10], as those tasks require lead equalization on the part of the human operator and typically involve control inputs involving nonlinear "pulsing" control inputs.[11] Figures 4 – 7 show the Bode diagrams for the pilot transfer functions and Figs. 8-11 show the corresponding Bode diagrams for the open-loop pilot/vehicle transfer functions θ/θ_e. As Figs. 8 - 11 indicate the crossover model of the human pilot is in evidence in the four tasks.[10] From Figs 4–11 the desired information about fundamental pilot equalization and crossover frequencies is easily obtained. The large discrepancies that appear with respect to initial estimates in some parameter identifications, e.g., K3 and K4 do not necessarily indicate poor identification, but rather the identification procedure accommodating the Y_{PF} changes through the template of Eq. 14.

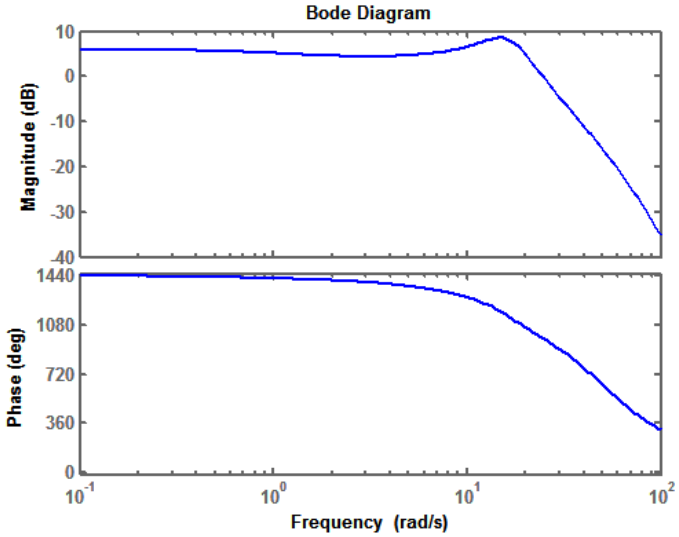

Figure 4 Bode diagram of Structural Model fit for pilot, Task 1.

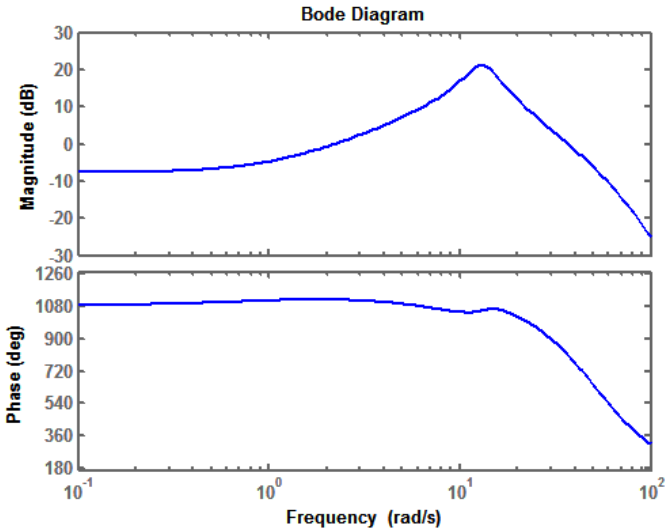

Figure 5 Bode diagram of Structural Model fit for pilot, Task 2.

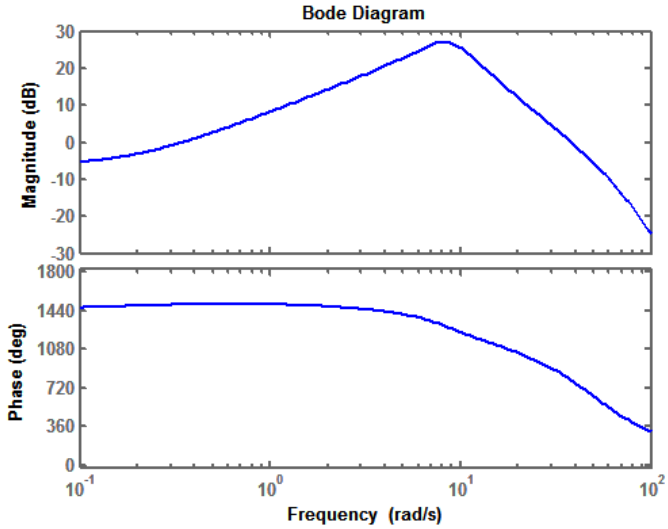

Figure 6 Bode diagram of Structural Model fit for pilot, Task 3.

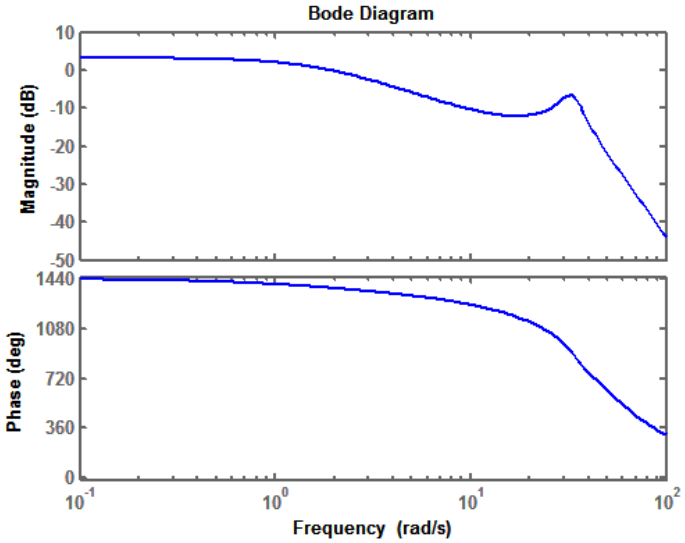

Figure 7 Bode diagram of Structural Model fit for pilot, Task 4.

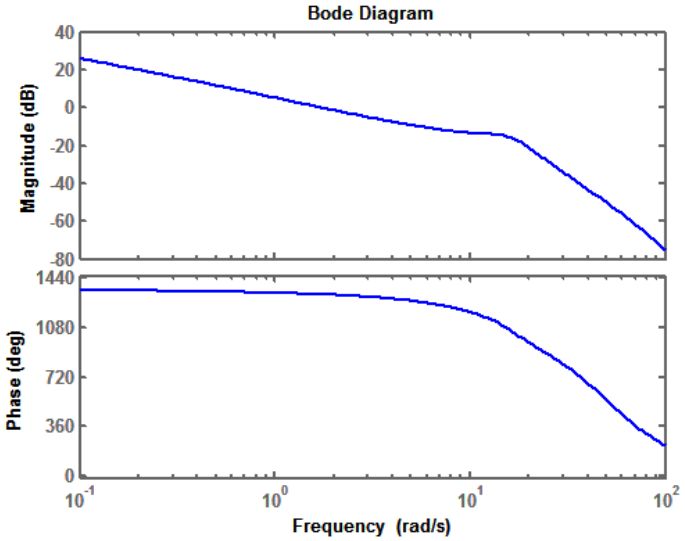

Figure 8 Bode diagram of open loop pilot/vehicle transfer function using Structural Model fit, Task 1.

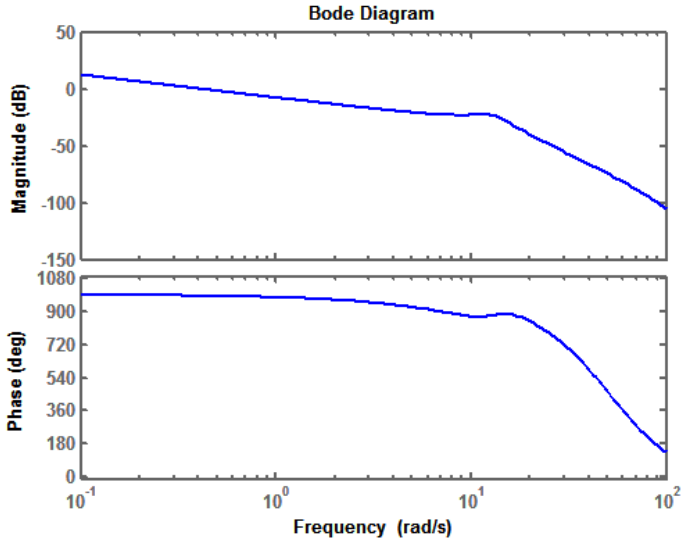

Figure 9 Bode diagram of open loop pilot/vehicle transfer function using Structural Model fit, Task 2.

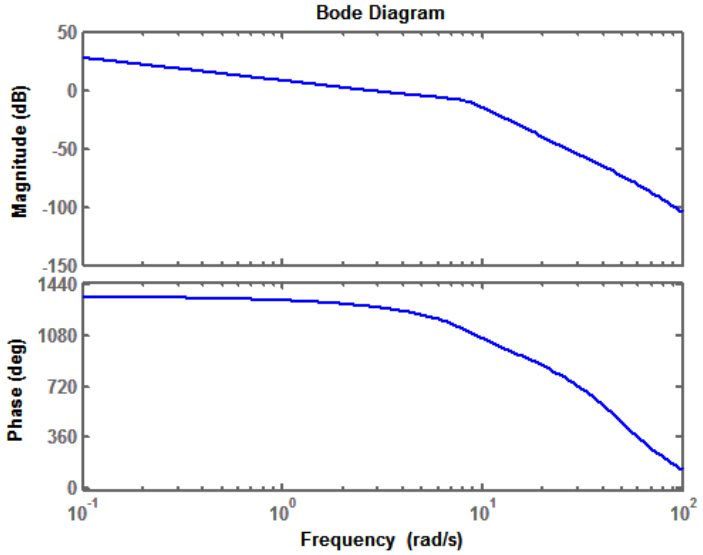

Figure 10 Bode diagram of open loop pilot/vehicle transfer function using Structural Model fit, Task 3.

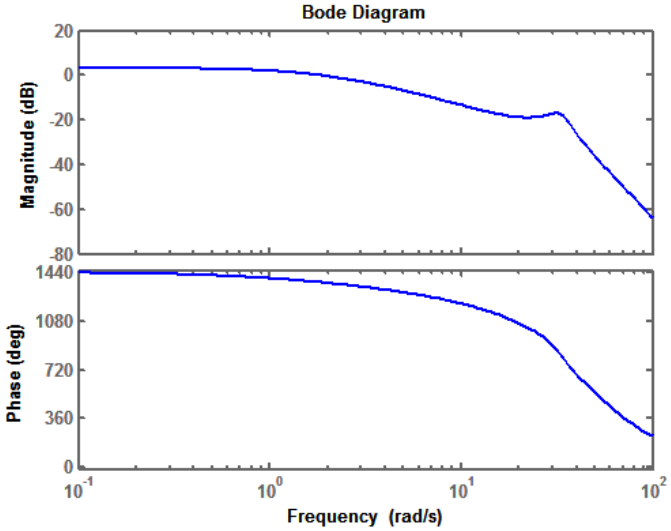

Figure 11 Bode diagram of open loop pilot/vehicle transfer function using Structural Model fit, Task 4.

Figures 12 – 14 show model and experimental fits to frequency-domain measures of pilot dynamics from Ref. 12, for controlled elements equivalent (or nearly so) to those of Tasks 1, 3 and 4 of Eqs. 13. The similarity among these and those of Figs. 4, 6 and 7 is worthy of note.

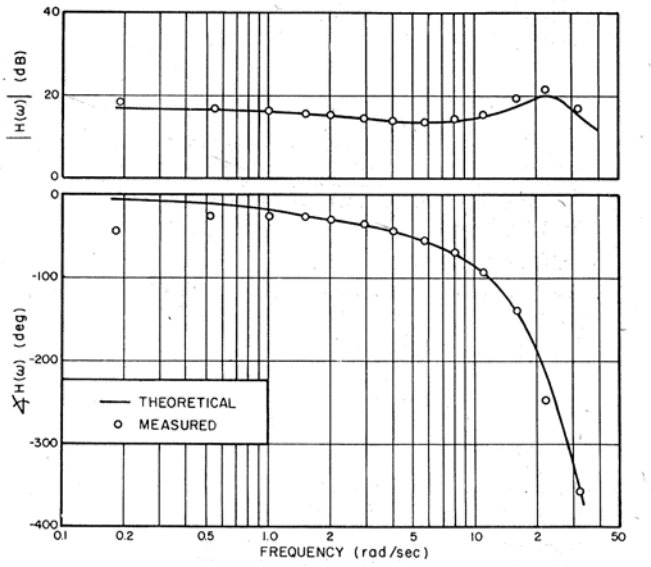

Figure 12 Bode diagram of measured and model-generated human operator Transfer functions for Y_c = K/s from Ref. 12.

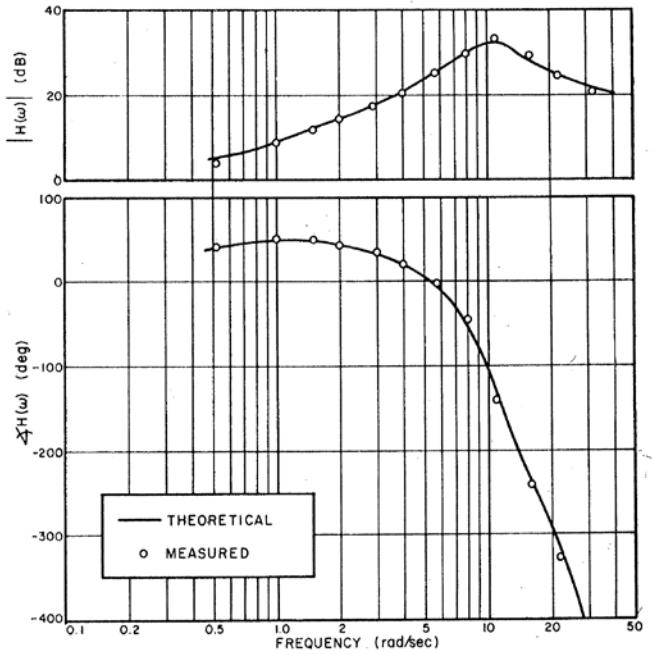

Figure 13 Bode diagram of measured and model-generated human operator Transfer functions for $Y_c = K/s^2$ from Ref. 12.

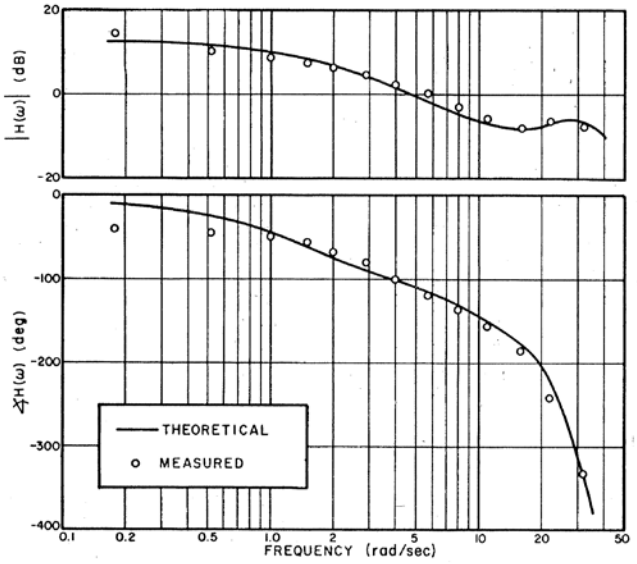

Figure 14 Bode diagram of measured and model-generated human operator Transfer functions for $Y_c = K/(s+40)$ from Ref. 12.

IV. Handling Qualities Estimation

A. The Handling Qualities Sensitivity Function (HQSF)

The research summarized in Refs. 2, 5, and 14 demonstrated the utility of a Handling Qualities Sensitivity Function (HQSF) in predicting piloted aircraft handling qualities levels. Referring to Fig. 3, the HQSF is defined as

$$\text{HQSF} = \left| \frac{1}{K_P} \frac{U_M}{C} (j\omega) \right| \tag{18}$$

with the open-loop crossover frequency adjusted to 2 rad/sec. Figure 15, from Ref. 13 shows a typical HQSF result.

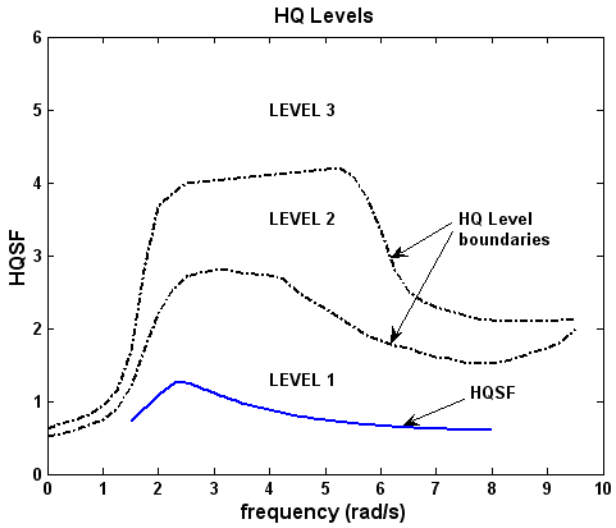

Figure 15 Typical HQSF results showing predicted Level 1 handling qualities from Ref. 13.

B. HQSF Calculations for Four Tasks of Section III

The work of the previous section suggests an approach in which identified Structural Model parameters (along with a model of the vehicle being controlled) for a specific vehicle and task can be used to create the HQSF based upon tracking data. Figure 16 and 17 show the HQSFs for the tasks 1 and 3 analyzed in the preceding section. These represent the easiest (Task 1) and most difficult (Task 3) of the four tasks.[15] The only modification that occurred was to change the identified gain value K_p = K1 so that the open-loop crossover frequency of the pilot/vehicle model was 2 rad/sec, as required by the HQSF procedure of Refs. 2 and 5. The HQSFs clearly show a sharp degradation in handling qualities between Task 1 and Task 3. Task 3, however, is still rated Level 1 which is far too conservative for this controlled element. For example, the ratings given to controlled elements similar to this in Ref. 15 averaged approximately 7.4/10 on the Copper-Harper rating scale, (including a number of Cooper-Harper "10s") clearly indicating Level 3 handling qualities. This can be partially attributed to the aforementioned nonlinear "pulsing" control activity that typically accompanies human control of second-order controlled elements. This behavior is shown in Fig. 18. References 2 and 5 accommodate this activity in calculating the HQSF by operating upon U_M and C, i.e., by calculating Finite Fourier Transforms of each and then forming the appropriate ratio given Eq. 18. Here, a slightly different tack is taken. Using the identified K1 – K4 gains, and the time histories of tracking error θ_e and operator control inputs δ_M, the signal UM is created and the HQSF transfer function magnitude is obtained by the identification technique offered in Ref. 16. The result of such calculations for this Task 3 is shown in Fig. 19 where Level 3 Handling Qualities Levels are now clearly indicated.

The reader is finally reminded that only one simulation run was conducted for these tasks. A far better approach, of course, would be to average the "identified" HQSFs over a series of runs. The reader is again reminded that only 30 sec of tracking data were used in the identification procedure, itself, with the final 30 sec used to calculate the VAF.

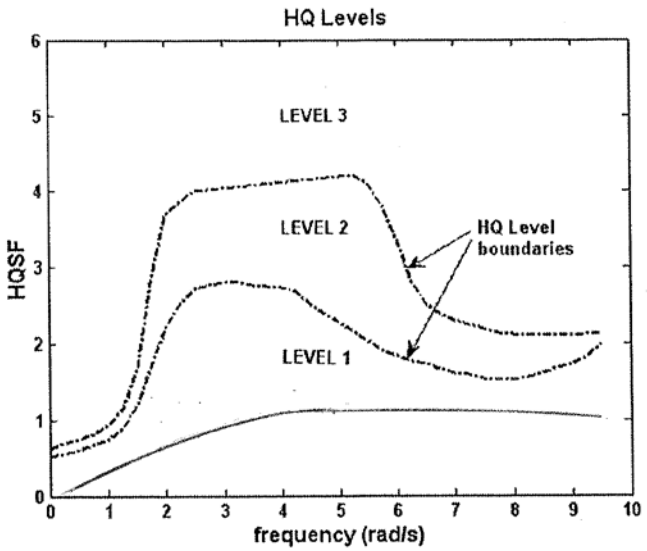

Figure 16 HQSF for Task 1.

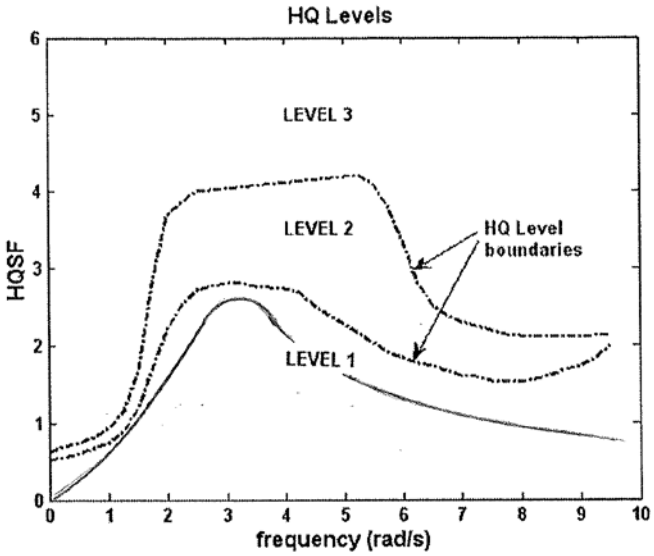

Figure 17 HQSF for Task 3.

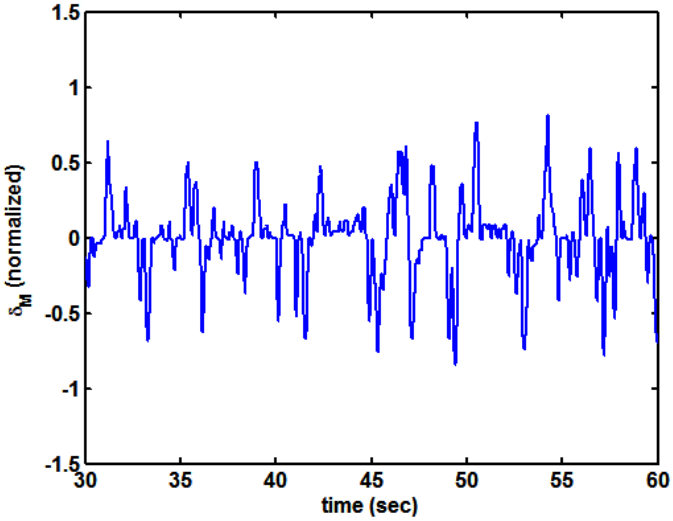

Figure 18 Pulsive operator control behavior in Task 3.

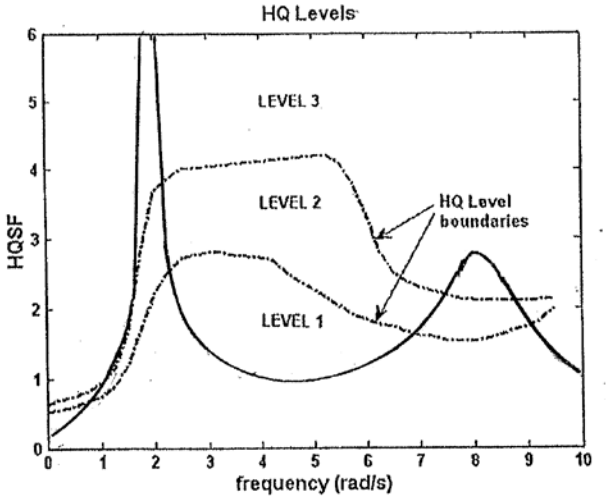

Figure 19 HQSF obtained from identified Structural Model parameters, including effects of nonlinearities, Task 3.

V. Tracking Examples with Aircraft Dynamics

A. Vehicle and Tracking Task

Using a vehicle model described in Ref. 2, a longitudinal tracking task was conducted. The aircraft chosen for simulation is shown in Fig. 20, a Boeing 747. The aerodynamic model was taken from Ref. 17 and the flight conditions considered is indicated in Table 4. As in the study of Section III, the identification results are based upon a single run of a well-trained subject. The RMS value of the pitch-attitude command was 0.75 deg. To repeat a statement in Section III, the purpose of the study was to demonstrate the general utility of the identification approach rather than a detailed description of operator dynamics. Also, as in the tasks of Section III, a 60 sec run was completed with the first 30 sec devoted to identification and the last 30 sec to evaluation of the VAF.

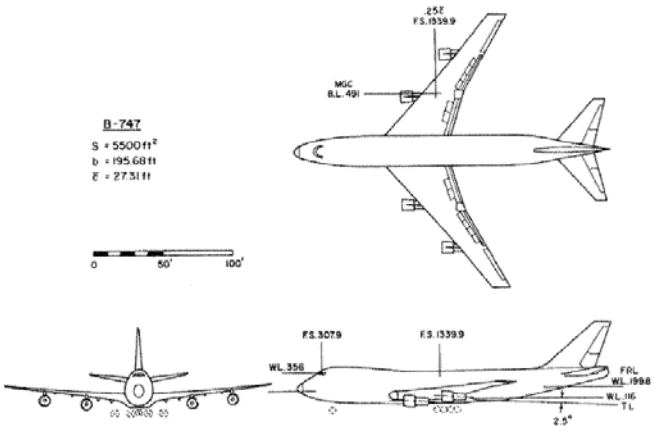

Figure 20 The Boeing 747 aircraft from Ref. 17.

Table 4 Flight Conditions for Aircraft of Fig. 20

Flight Condition 6	
Altitude (ft)	20,000
Airspeed (ft/sec)	674
Configuration	gear up, 0 deg flaps

A rate-command stability and command augmentation system (SCAS) was included as described in Ref. 2, and included auto-throttles and rate and amplitude-limited elevator actuators. The vehicle model for longitudinal control was of 13th order. A longitudinal pitch-attitude tracking task similar to that used in the experiments in Section IIIA was employed. The sum of sinusoids input of Table 1 was used in the pitch-attitude tracking task as was the display of Fig. 2. Initial estimates of the Structural Pilot Model parameters for both flight configurations are shown in Table 5.

Table 5 Initial Estimates for Structural Model Parameters for Flight Condition 6

$K_1 = 4.37, K_2 = 0.619, \quad K_3 = 2.0, \; K_4 = 20.$

B. Identification Results

Table 6 shows the identified Structural Model gain values along with the VAF values for the flight condition. Figures 21 and 22 show the Bode diagrams of the Structural Model fit and that of the corresponding open-loop transfer function.

Table 6 Identified Structural Model Parameters and VAF

K_i	VAF
$K_1 = 1.76$ $K_2 = 0.754$ $K_3 = 0.0188$ $K_4 = 1.07$	0.64

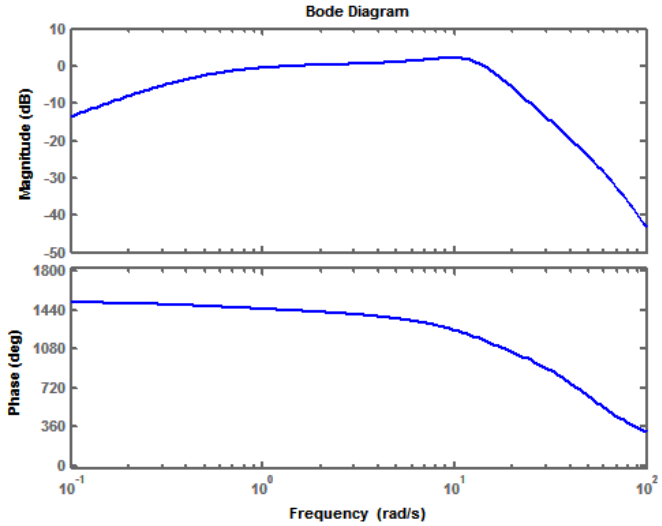

Figure 21 Bode diagram of Structural Model fit for pilot, Flt. Cond. 6.

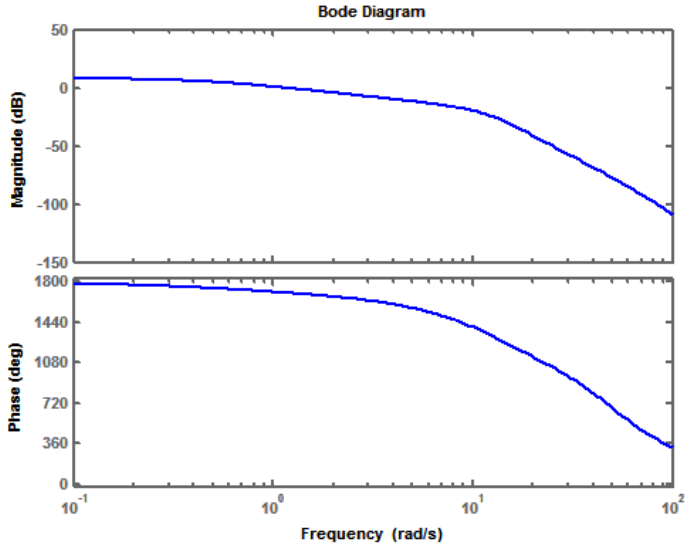

Figure 22 Bode diagram of open loop pilot/vehicle transfer function using Structural Model fit, Flt. Cond.6.

Figure 23 is a comparison of pitch-attitude from human-in-the-loop simulation, and that obtained when the identified pilot model replaces the human.

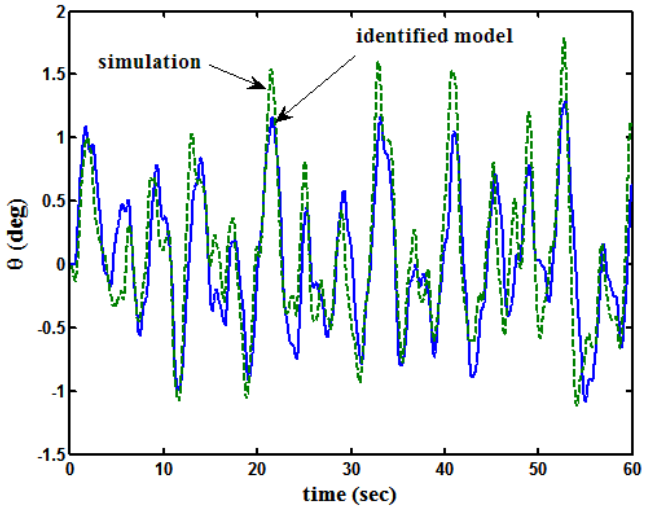

Figure 23 Comparison of pitch-attitude with human-in-the-loop and the identified model.

C. Identification-Based HQSF

Using a value of K1 that would yield a 2 rad/sec crossover frequency, Fig. 24 shows the HQSFs for Flt. Cond. 6. The general similarity between the HQSFs of Figs. 16 and 24 is explained by the fact that the "effective vehicle" in each case exhibited K/s-like pitch-attitude characteristics over a broad frequency range[2], dynamics of which have long been associated with desirable handling qualities.[15]

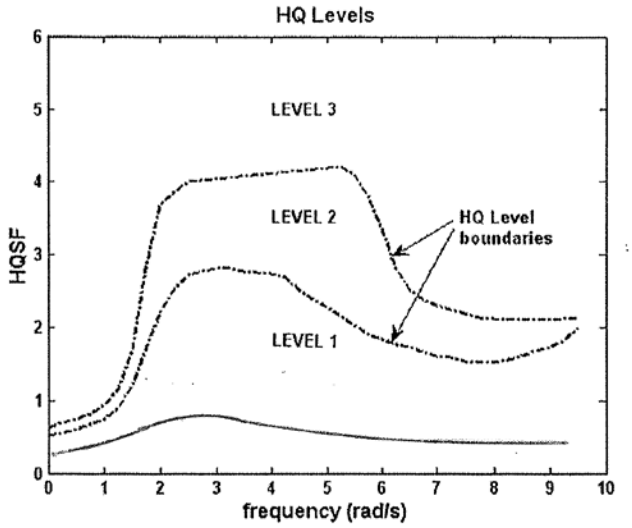

Figure 24 HQSF obtained from identified Structural Model parameters, Flt. Cond. 6.

Some limited elevator actuator rate saturation (± 60 deg/sec) occurred during the tracking task for Flt. Cond. 6 as shown in Fig. 25. It was of interest to determine whether this limiting affected the HQSF. The identification technique of Section IIIB was again applied with the results shown as the dashed curve in Fig. 26 and compared to that of Fig. 24. As can be seen, little change is noted. The degradation that is seen can be attributed to the fact that actuator rate limiting is accompanied by an

additional effective time delay in the vehicle dynamics.[18] The fact that measured pitch-attitude is used in generating the estimate of UM/C means that the effects of any additive time delays are included in the HQSF.

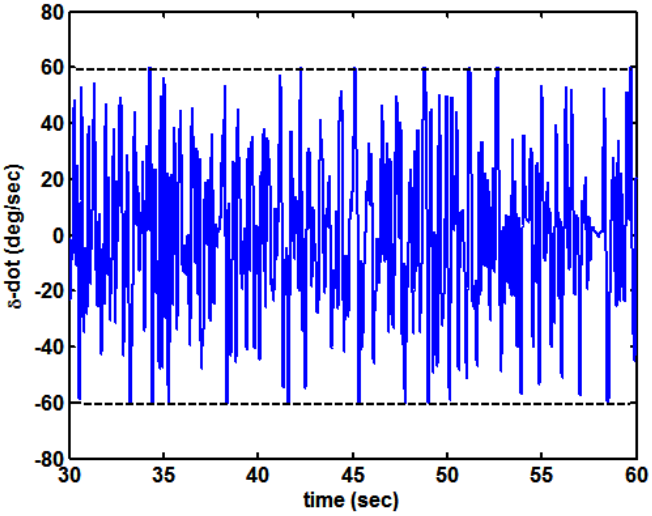

Figure 25 Elevator actuator rate limiting, Flt. Cond. 6

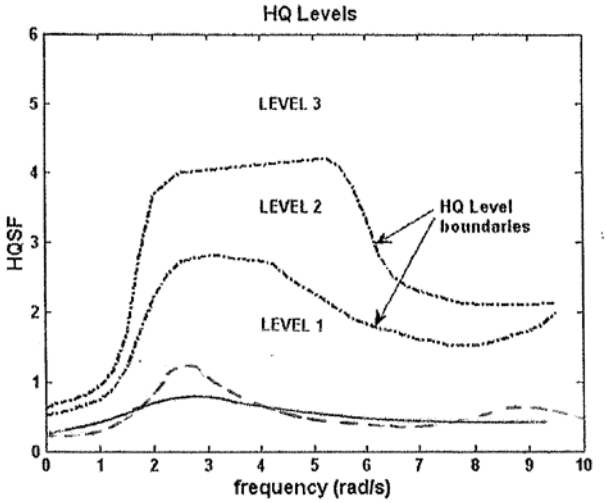

Figure 26 HQSF obtained from identified Structural Model parameters, including effects of rate limiting, Flt. Cond. 6.

VI. Multiple Run Results with Aircraft Dynamics

A. Identification Results

A series of 10 additional runs were completed with the Boeing 747 model at Flight Condition 6. As before, the runs were 60 sec in length with the first 30 sec devoted to Structural Model parameter estimation and the last 30 sec devoted to calculating the VAF. The estimates for the single identification of Table 6 were also included, making a total of 11 runs. Initial parameter estimates were identical to those of Table 5. Table 7 summarizes the identification results.

Table 7 Identified Structural Model Parameters and VAF

Parameter	Mean	Std. Dev.	VAF	
			Mean	Std. Dev.
K1	4.35	2.77		
K2	1.79	1.82		
			0.52	6.7
K3	0.589	0.417		
K4	3.31	2.71		

The reader will note the large standard deviations of the parameter estimates. This is not necessarily a sign of poor identification, but rather that a wide range of parameter values may be adopted by the human without performance penalties. Figure 27 and 28 show the Bode diagrams for the pilot transfer function and the open-loop pilot/vehicle transfer function using the mean parameter values of Table 7.

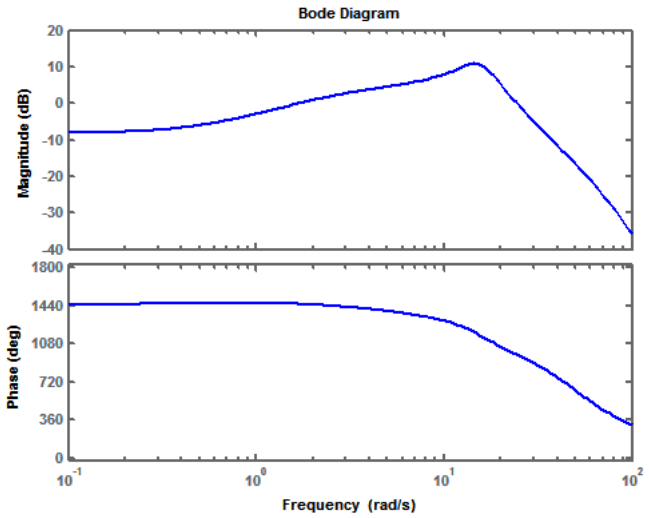

Figure 27 Bode diagram of Structural Model fit for pilot using mean parameter estimates, Flt. Condition 6.

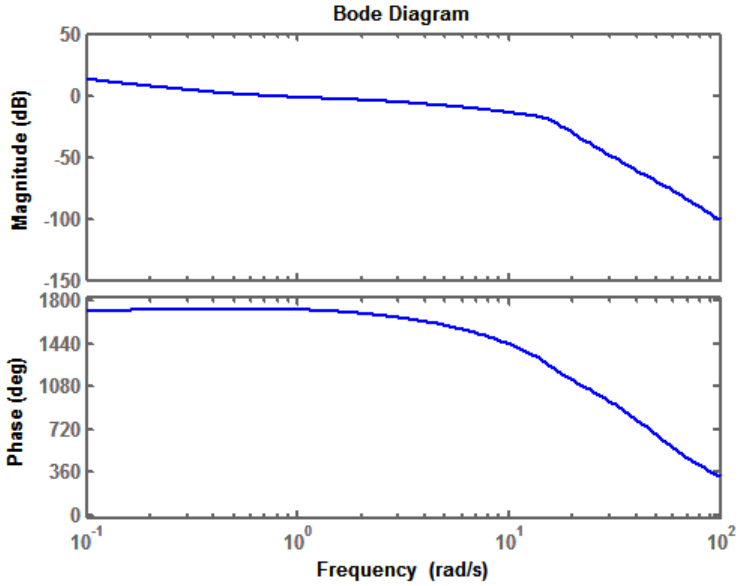

Figure 28 Bode diagram of open loop pilot/vehicle transfer function using mean parameter estimates, Flt. Cond. 6.

Comparing Figs. 21 and 27, one sees some effective lead generation in the latter figure. This may be attributable to the pilot compensating for the time delay created by the actuator rate limiting.[18] This behavior has been documented in the experiments of Ref. 19.

B. HQSF Calculation

Figure 29 shows the corresponding HQSF using the mean parameter estimates. Comparing Figs. 24 and 29 emphasizes the importance of using multiple runs in handling qualities estimation. The poorer handling qualities predicted in the HQSF in Fig .29 can be attributed to the necessity of modest lead equalization evident in Fig. 27.

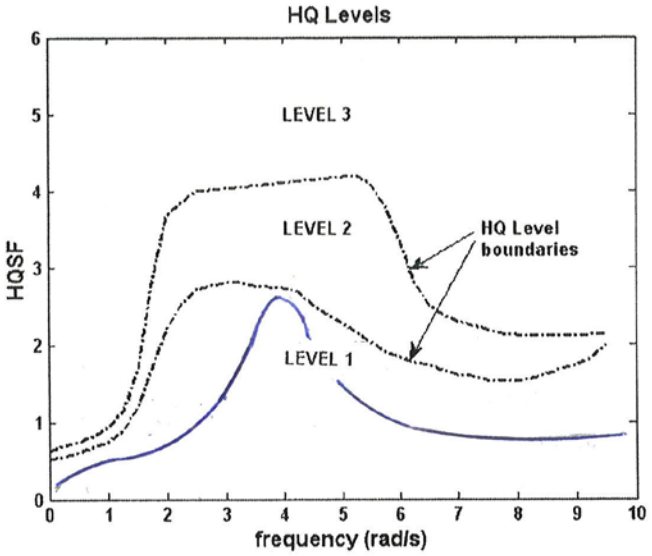

Figure 29 HQSF obtained from mean parameter estimate, Flt. Cond. 6.

VII. Discussion

It cannot be overemphasized that the purpose of this limited study was not the development of a novel tool for precise, broad-frequency identification of human pilot dynamics. Other approaches, such as the maximum likelihood technique offered in Ref. 20, or the Automated Parameter Identification Technique (APID) offered in Ref. 21 provide such capabilities. Rather the approach espoused is intended as a preliminary step in allowing the simulation engineer to make approximate but useful determination of the basic equalization characteristics being employed by the human pilot and to do so in the framework of a specific pilot model, i.e., the Structural Model of the human pilot. As such, the technique may serve as an experimental complement to the analytical approach espoused in Ref. 2. Finally, the inclusion of vestibular cueing in the Structural Model, absent in the simple fixed-base tracking study conducted herein, should be considered.

VIII. Conclusions

Based upon the preliminary, exploratory study summarized herein, the following conclusions can be drawn.

(1) A time-domain identification technique can be applied to the estimation of a limited, but important set of parameters defining the equalization characteristics of the human operator/pilot.
(2) The technique can determine the fundamental equalization characteristics of the human pilot in well-defined tracking tasks.
(3) The technique may allow the estimation of an important handling qualities predictive metric, the handling qualities sensitivity function, directly from simulation data, including approximating the effects of nonlinearities.
(4) More research is obviously needed in validating the approach with a larger set of simulation tracking data.

Acknowledgment

This research was supported by NASA Ames Research Center through the University Affiliated Research Center, (UARC), University of California – Santa Cruz. The Task Requestor was Dr. Barbara Sweet of NASA Ames Research Center. The Task Order Manager was Dr. Bassam Mussafar.

References

[1]Hess, R. A., "A Preliminary Study of Human Pilot Dynamics in the Control of Time-Varying Systems," AIAA Paper No. 2011-6554, AIAA Modeling and Simulation Technologies Conference, Aug. 8-11, 2011, Portland, OR.

[2]Hess, R. A., and Joyce, R., "Analytical Investigation of Transport Aircraft Handling Qualities," submitted for presentation at the 2013 AIAA Atmospheric Flight Mechanics Conference, Aug. 9-12, Boston, MA.

[3]Moore, J. K., "Human Control of a Bicycle," Ph.D. Dissertation, Dept. of Mechanical and Aerospace Engineering, University of California, Davis, 2012.

[4]Hess, R., Moore, J. K., and Hubbard, M., "Modeling the Manually Controlled Bicycle," *IEEE Transactions on Systems, Man, and Cybernetics, Part A: Systems and Humans*, Vol. 42, No. 3, 2012, pp. 545-557.

[5]Hess, R. A., "Unified Theory for Aircraft Handling Qualities and Adverse Aircraft-Pilot Coupling," *Journal of Guidance, Control, and Dynamics*, Vol. 20, No. 6, 1997, pp. 1141-1148.

[6]Ljung, L., *System Identification: Theory for the User*, Prentice Hall, 1998.

[7]Bekey, G. A., Meissinger, H. F., and Rose, R. E., "A Study of Model Matching Techniques for the Determination of Parameters in Human Pilot Models," NASA CR-143, 1965.

[8]Taylor, L. W., Jr., "Nonlinear Time-Domain Models of Human Controllers," *Journal of Optimization Theory and Applications*, Vol. 5, No. 1, 1970, pp. 23-37.

[9]Hess, R. A., Zeyada, Y., "Pilot/Vehicle Dynamics, Nonlinear, - An Interactive Computer Program for Modeling the Human Pilot in Single-Axis linear and Nonlinear Tracking Tasks," Dept. of Mechanical and Aeronautical Engineering, 1999.

[10]McRuer, D. T. and Krendel, E. S., "Mathematical Models of Human Pilot Behavior," AGARDograph No. 188, 1974.

[11]Hess, R. A., "A Rationale for Human Operator Pulsive Control Behavior," *Journal of Guidance, and Control*, Vol. 2, No. 3, 1979, pp. 221-227.

[12]Kleinman, D. L., and Levison, W. H., "An Optimal Control Model of Human Behavior," *Proceedings of the Fifth Annual NASA-University Conference on Manual Control,"* 1969, pp. 343-366.

[13]Hess, R. A., "Frequency-Domain Design/Analysis of Robust Flight Control Systems," in *System Control Technologies, Design considerations & Integrated Optimization Factors for Distributed nano Unmanned Air Vehicle (UAV) Applications*, NATO Lecture Series RTO-EN-SCI-175. 2007, pp. 3-1 to 3-55.

[14]Anon., "Flight Control Design – Best Practices," RTO-TR-029, Dec. 2000.

[15]McDonnell, J. D., "Pilot Rating Techniques for the Estimation and Evaluation of Handling Qualities," AFFDL-TR-68-76, 1968.

[16]Hess, R. A., "A Preliminary Study of Human Pilot Dynamics in the Control of Time-Varying Systems," AIAA Paper No. 2011-6554, AIAA Modeling and Simulation Technologies Conference, 8- ll August, 2011, Portland, OR.
[17]Heffley, R. K., and Jewell, W. F., "Aircraft Handling Qualities Data," NASA CR-2144, 1972.
[18]Klyde, D. H., and Mitchell, D. G., "Investigating the Role of Rate Limiting in Pilot-Induced Oscillations," *Journal of Guidance, Control, and Dynamics*, Vol. 27, No. 5, 2004, pp. 804-813.
[19]Hess, R. A., "The Effects of Time Delays on Systems Subject to Manual Control," *Journal of Guidance, Control, and Dynamics*, Vol. 7, No. 4, 1984, pp. 416-421.
[20]Zaal, P., and Sweet, B., "Identification of Time-Varying Pilot Control Behavior in Multi-Axis Control Tasks," AIAA Paper No. 2012-4793, AIAA Modeling and Simulation Technologies Conference, Minneapolis, MN, 2012.
[21]Zaychik, K. B., and Cardullo, F. M., "Intelligent Systems Approach for Automated Identification of Individual Control Behavior of a Human Operator," NNASAS/CR-2012-217555.